



Quantitative estimation of hourly precipitation in the Tianshan Mountains based on area-to-point kriging downscaling and satellite-gauge data merging

Xin-yu LU, Yuan-yuan CHEN, Guo-qiang TANG, Xiu-qin WANG, Yan LIU, Ming WEI

View online: <https://doi.org/10.1007/s11629-021-6901-5>

Articles you may be interested in

[Precipitation scale effect of the TRMM satellite in Tianshan, China](#)

Journal of Mountain Science. 2023, 20(5): 1349 <https://doi.org/10.1007/s11629-022-7714-x>

[Ground validation of Fengyun-4A and Global Precipitation Measurement satellite observations over an alpine and canyon basin of the southeastern Tibetan Plateau](#)

Journal of Mountain Science. 2022, 19(12): 3568 <https://doi.org/10.1007/s11629-022-7451-1>

[Disintegration of uncertainties associated with real-time multi-satellite precipitation products in diverse topographic and climatic area in Pakistan](#)

Journal of Mountain Science. 2021, 18(3): 716 <https://doi.org/10.1007/s11629-020-6168-2>

[Estimation of mountain block recharge on the northern Tianshan Mountains using numerical modeling](#)


Journal of Mountain Science. 2021, 18(7): 1794 <https://doi.org/10.1007/s11629-020-6589-y>



[Evaluation of spatiotemporal variability of temperature and precipitation over the Karakoram Highway region during the cold season by a Regional Climate Model](#)



Journal of Mountain Science. 2020, 17(9): 2108 <https://doi.org/10.1007/s11629-019-5772-5>


Original Article


Quantitative estimation of hourly precipitation in the Tianshan Mountains based on area-to-point kriging downscaling and satellite-gauge data merging


LU Xin-yu^{1,2}  <https://orcid.org/0000-0001-5874-3163>; e-mail: luxy0322@126.com

CHEN Yuan-yuan^{3*}  <https://orcid.org/0000-0002-0892-0771>;  e-mail: yuanchen91@163.com

TANG Guo-qiang^{4,5*}  <https://orcid.org/0000-0002-0923-583X>;  e-mail: guoqiang.tang@usask.ca

WANG Xiu-qin¹  <https://orcid.org/0000-0002-2526-7954>; e-mail: xiuqinwang66517330@163.com

LIU Yan¹  <https://orcid.org/0000-0003-0935-8669>; e-mail: liuyan@idm.cn

WEI Ming⁶  <https://orcid.org/0000-0002-9328-6153>; e-mail: njueducn@126.com

* Correspondence

¹ Institute of Desert Meteorology, China Meteorological Administration, Urumqi 830002, China

² Central-Asia Research Center of Atmosphere Science, Urumqi 830002, China

³ College of Environment, Zhejiang University of Technology, Hangzhou 310014, China

⁴ University of Saskatchewan Coldwater Lab, Canmore T1W 3G1, Canada

⁵ Center for Hydrology, University of Saskatchewan, Saskatchewan S7N 5A2, Canada

⁶ Collaborative Innovation Center on Forecast and Evaluation of Meteorological Disasters, Nanjing University of Information Science & Technology, Nanjing 210044, China.

Citation: Lu XY, Chen YY, Tang GQ, et al. (2022) Quantitative estimation of hourly precipitation in the Tianshan Mountains based on area-to-point kriging downscaling and satellite-gauge data merging. *Journal of Mountain Science* 19(1). <https://doi.org/10.1007/s11629-021-6901-5>

© Science Press, Institute of Mountain Hazards and Environment, CAS and Springer-Verlag GmbH Germany, part of Springer Nature 2022

Abstract: Precipitation, a basic component of the water cycle, is significantly important for meteorological, climatological and hydrological research. However, accurate estimation on the precipitation remains considerably challenging because of the sparsity of gauge networks and the large spatial variability of precipitation over mountainous regions. Moreover, meteorological stations in mountainous areas are often dispersed and have difficulty in accurately reflecting the intensity and evolution of precipitation events. In this study, we proposed a novel method to produce high-quality,

high-resolution precipitation estimates in the Tianshan Mountains, China, based on area-to-point kriging (ATPK) downscaling and a two-step correction, i.e., probability density function matching-optimum interpolation (PDF-OI). We obtained 1-km hourly precipitation data in the Tianshan Mountains by merging estimates from the Integrated Multi-satellite Retrievals for Global Precipitation Measurement (IMERG) product with observations from 1065 meteorological stations in the warm season (May to September) during 2016–2018. The spatial resolution and accuracy of the merged precipitation data greatly increased compared to IMERG. According to a cross-validation with gauged observations, the correlation coefficient (CC),

Received: 20-May-2021

1st Revision: 01-Jul-2021

2nd Revision: 26-Sep-2021

Accepted: 20-Oct-2021

probability of detection (POD) and critical success index (CSI) increased from 0.30, 0.50 and 0.24 for IMERG to 0.63, 0.65 and 0.38, respectively, for the merged estimates, and the root mean squared error (RMSE), mean error (ME) and false alarm ratio (FAR) decreased from 0.46 to 0.38 mm/h, 0.06 to 0.05 mm/h and 0.69 to 0.52, respectively. The proposed method will be useful for developing high-resolution precipitation estimates in mountainous areas such as central Asia and the Belt and Road Initiative regions.

Keywords: Hourly precipitation; Downscaling; merging; Tianshan Mountains; IMERG; Area-to-point kriging (ATPK)

1 Introduction

As a basic component of the water cycle of Earth, precipitation plays an important role in the fields of meteorology, climatology and hydrology (Kidd and Human 2011). High-resolution and high-quality precipitation data serve as the basis of mesoscale numerical weather prediction models and hydrological monitoring forecasts and have not only been utilized to test modern models of high-resolution numerical weather forecasts but also provided critical information for monitoring meso- and small-scale precipitation events and preventing disasters caused by these events, such as mountain torrents, landslides and debris flows (Yu et al. 2013; Han et al. 2021).

Currently, precipitation observations are acquired in three main ways, i.e., rain gauges, ground-based radar and satellite remote sensing. Although station observations can be highly accurate, most stations are unevenly dispersed in low-altitude regions, and thus, the observation data are insufficiently representative. In contrast, weather radar-based precipitation data calculated based on the reflectivity factor and rainfall intensity ($Z-I$) relationship have a certain advantage in regional estimations. However, the $Z-I$ relationship can vary greatly according to precipitation systems, seasons and regions, which affects the accuracy of radar-predicted precipitation. In addition, radar detection is sensitive to surface obstructions, beam effects and velocity ambiguity, and therefore, the use of this method remains greatly restricted in practice. As another alternative, remote sensing and geographic information systems have rapidly developed,

providing new approaches for large-scale synchronous precipitation observations (Chen et al. 2017; Han et al. 2019). Satellite-derived precipitation products have the unique merits of being suitable under all weather conditions, having global coverage and reflecting the spatial distribution of precipitation; hence, these products are valuable for understanding global and regional precipitation distributions, as well as precipitation variations. However, satellite precipitation products usually have unsatisfactory spatial resolutions and low accuracy due to the limitations of the physical principles and algorithms used for retrieving satellite-based precipitation. Therefore, satellite-based precipitation products must be calibrated and downscaled prior to their application (Zheng et al. 2018; Kiyomars et al. 2018; Yang et al. 2020).

Considering the unsatisfactory spatial resolution of satellite precipitation products, a number of statistical downscaling methods have been proposed in recent years. By constructing statistical models linking low-resolution satellite precipitation with high-spatial-resolution environmental data, such as topography and vegetation, satellite precipitation data can be downscaled. However, due to its cumulative effects, precipitation presents more significant statistical correlations with environmental variables at the monthly and annual scales than at the daily and hourly scales, where the influence of weather processes becomes more noticeable (Yang and Luo 2014a; Lu et al. 2018). To date, most studies on satellite precipitation product downscaling have focused on the monthly and annual scales (Immerzeel et al. 2009; Jia et al. 2011; Xu et al. 2015; Ma et al. 2017; Chen et al. 2018; Zhang et al. 2018). However, for land hydrological simulations, weather forecasting and the monitoring of mountain floods and geological disasters, hourly precipitation monitoring at this weather scale is far more important than the large time scale precipitation (Shen et al. 2018).

Some studies have developed methods to merge satellite precipitation data with observations to improve the quality of satellite precipitation products. These methods include objective statistical analysis (Boushaki et al. 2009), optimum interpolation (OI) (Xie and Xiong 2011; Shen et al. 2014; Wu et al. 2018; Tang et al. 2021), dual-core smoothing (Li and Shao 2010), geographical difference analysis (Baik et al. 2016; Xu et al. 2015), Bayesian models (Chiang et al. 2021), machine learning (Zhang et al. 2021), and

generative adversarial networks (GANs) (Wang et al. 2021). Although these merging methods increase the precision of precipitation estimates to some extent, they tend to directly merge satellite precipitation data and rain gauge-based observation data on considerably different scales, which inevitably introduces large errors in data merging (Park et al. 2017; Verdin et al. 2015). Due to the discontinuity of the background field, direct merging results in remarkable deviations along the grid boundary of the original satellite precipitation data (Li and Shao 2010). To solve this data mismatch problem, Kyriakidis (2004, 2005) proposed a geostatistical downscaling method, i.e., area-to-point kriging (ATPK), which has an important feature: interpolation downscaling to the average of the sum of all points in a given area is equivalent to the original value of the given area. Over the past decade, ATPK has undergone rapid development and has been applied in various fields (Liu et al. 2008; Goovaerts 2010; Kerry et al. 2012; Wang et al. 2015; Zhang et al. 2017; Jin et al. 2018, Park et al. 2017; Chen et al. 2018).

Due to the sparse distribution of rain gauges and the considerable errors of radar quantitative precipitation estimation, precipitation estimation over mountainous areas has always been a challenge. Previous studies mostly used a limited number of rain gauges over mountainous regions to correct the deviation of satellite precipitation or radar quantitative precipitation estimation through multiple linear regression, geographic information systems, neural networks and other methods (Gjertsen and Dahl 2002; Marquinez et al. 2003; Yin et al. 2004, 2008; Qi et al. 2010; Yang and Luo 2014b; Nan et al. 2018; Arulraj et al. 2019). Considering that spaceborne radar measurements are much less affected by the mountain blocking and beam broadening effect in the vertical direction, incorporation of space-based radar information into a ground-based radar network can improve the understanding of the precipitation rate and precipitation type in mountainous areas (Wen et al. 2014). In this study, we performed experiments on the Integrated Multi-satellitE Retrievals for Global Precipitation Measurement (IMERG) hourly precipitation products, which were expected to provide high-spatiotemporal-resolution precipitation data for studying the mechanisms underlying the development of meso- and small-scale weather systems. The introduction of ATPK increased the

spatial resolution of the satellite precipitation data without forfeiting the original information, which not only achieved downscaling for the satellite precipitation products but also secured a better match between the satellite precipitation data and observed observations, thereby laying a satisfactory data foundation for further merging. Furthermore, the probability density function and OI (PDF-OI) approach was used to merge the observed precipitation data with post-downscaling satellite precipitation to obtain the final precipitation grid dataset with an increased spatial resolution and a higher accuracy. This study may provide a new reference for researching the generation of high-spatiotemporal-resolution precipitation data in mountainous areas where precipitation data are lacking.

2 Study Area and Data

2.1 Study area

The Tianshan Mountains constitute the largest mountain range in central Asia. The part of this mountain range within the territory of China is located within 39°N–45°N and 73°E–96°E and traverses the whole region of Xinjiang (Fig. 1) from the border between China and Kyrgyzstan to the Xingxingxia Gobi. The mountains within China stretch 1700 km long from east to west, accounting for approximately two-thirds of the total length of the Tianshan Mountains, and are 250–350 km wide from north to south. The Tianshan Mountains are known as the "water tower of central Asia", as 65% of the rivers in Xinjiang originate therein; these mountains are both the main source of water resources in northern and southern Xinjiang and the main runoff-producing area in Xinjiang. The precipitation in the mountain area decreases gradually from northwest to southeast, and the precipitation on the northern slope is noticeably greater than that on the southern slope (Fig. 1b). The Tianshan Mountains are the climate watershed separating North and South Xinjiang and serve as an important natural barrier that affects the weather and ecological environment in Xinjiang and in the central and western regions of China.

2.2 IMERG satellite precipitation product

The GPM mission is the successor of the Tropical

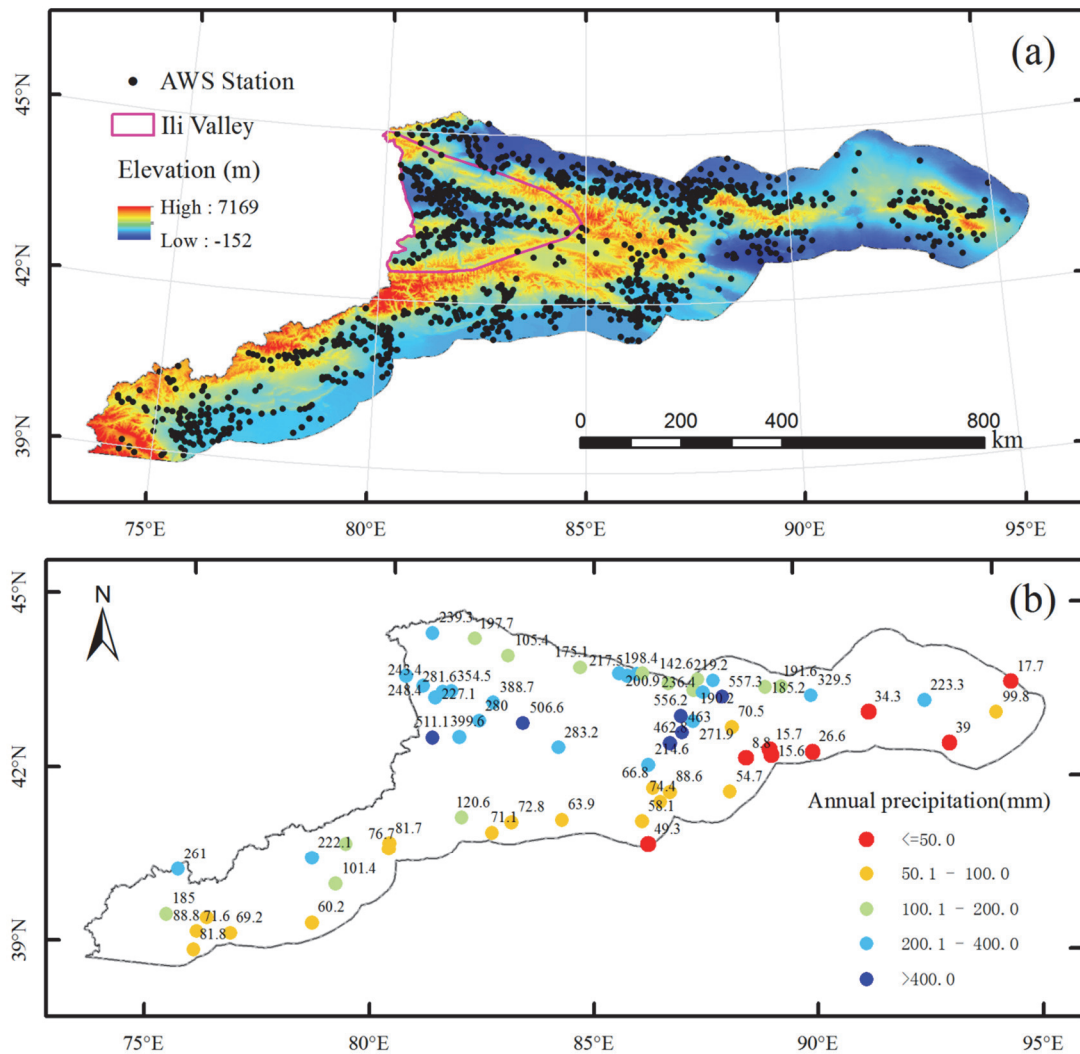


Fig. 1 Map of the Tianshan Mountains in China showing (a) the digital elevation model (DEM) and spatial distribution of automatic weather stations (AWSs) and (b) the annual precipitation at national stations.

Rainfall Measurement Mission (TRMM) carried out by the National Aeronautics and Space Administration (NASA) and Japan Aerospace Exploration Agency (JAXA). The purpose of the GPM mission is to provide new-generation global precipitation products with higher accuracy and higher resolution. GPM expands the sensor load of TRMM and enhances the precipitation observation capacity. The dual-frequency radar carried by the GPM Core Observatory (GPMCO) can detect the minimum echo intensity at the Ku band and adopts a high-sensitivity mode for interleaved sampling (Ka band). Furthermore, the microwave radiometer of the GPMCO has four more high-frequency bands than that of the TRMM satellite, which enhances the ability to observe traces of precipitation and solid precipitation. IMERG is the level-3 quasi-global GPM

grid product. A comparison of the GPM IMERG product with other commonly used satellite precipitation products in the Xinjiang region showed that IMERG overperformed other products in terms of precision, particularly at the hourly scale (Lu et al. 2018). Therefore, in this study, we used the “final-run” research-level IMERG precipitation product as the experimental data and selected the half-hourly precipitation between May and September (warm season) of 2016–2018 for downscaling and merging experiments.

2.3 Observed precipitation data

Hourly precipitation data observed by 1065 automatic weather stations (AWSs) (shown in Fig. 1) in the Tianshan Mountains were employed in this

study. The temporal range of these data is consistent with that of the IMERG precipitation data. The observed data were provided by the Information Center of the Xinjiang Meteorological Bureau and subjected to a series of quality controls, such as an extreme climate value test, a single-station extreme value test and a data consistency test. To ensure independence between calibration and merging, data from the 9 international exchange stations in the Tianshan Mountains participating in the IMERG “final-run” product were excluded. As AWSs stop working in the cold season, we selected the warm season (May to September) for this study. According to the results of 10-fold cross-validation, the stations were randomly divided into 10 groups according to altitude. This treatment was meant to ensure the representativeness of the training samples and validation samples (Tang et al. 2015; Lu et al. 2018).

3 Methodology

In this study, we performed downscaling and merging over the GPM IMERG hourly precipitation product. Specifically, the original half-hourly IMERG precipitation product was accumulated to the hourly scale and downscaled from the original 0.1° resolution to 0.01° (approximately 1 km) using ATPK interpolation. Then, PDF-OI was utilized to correct the system bias of the 1-km IMERG data and merge these data with the observed precipitation data. Finally, a cross-validation analysis is applied for validation, i.e., the AWSs were divided into 10 groups; 9 groups were selected each time, and 90% of the data were used for modeling. The remaining group contained 10% of the data to form an independent data set for accuracy verification of the merged products.

3.1 Downscaling of the IMERG hourly precipitation data

Considering the unsatisfactory resolution of satellite precipitation data, the half-hourly IMERG precipitation product was accumulated to the hourly scale and downscaled from the original 0.1° resolution to 0.01° using ATPK interpolation, which enabled the station data to be better matched with the satellite precipitation data. This processing further improved the merging effectiveness in the next step.

ATPK is a downscaling method that interpolates

unknown points with known data, where the estimate at an unknown point is the linear weighted sum of the data in its local area and nearby areas. The interpolation calculation is expressed as follows:

$$P_{sat}^{1km}(x) = \sum_{i=1}^n \lambda_i P_{sat}^{0.1^\circ}(v_i) \quad (1)$$

where $P_{sat}^{1km}(x)$ represents the precipitation at the 1-km predicted site, $P_{sat}^{0.1^\circ}(v_i)$ represents the low-spatial-resolution precipitation grid around the predicted site, λ_i is the weight coefficient of the low-resolution grid, and n represents the number of low-spatial-resolution pixels around the predicted site. Similar to that of common kriging interpolation, the weight coefficient of ATPK is determined by the minimal error variance in the precipitation at the predicted site. The detailed equation is defined as follows:

$$\sum_{j=1}^n \lambda_j \bar{C}(v_i, v_j) + \mu_x = \bar{C}(v_i, x), i = 1, 2, \dots, n \quad (2)$$

$$\sum_{j=1}^n \lambda_j = 1$$

where μ_x is the Lagrangian operator, which is used to control the unit sum of the weight coefficient λ_j , $\bar{C}(v_i, v_j)$ is the covariance between the low-spatial-resolution pixels v_i and v_j , and $\bar{C}(v_i, x)$ is the covariance between the low-spatial-resolution pixel v_i and the high-spatial-resolution pixel x . $\bar{C}(v_i, v_j)$ and $\bar{C}(v_i, x)$ can be calculated using the following equations:

$$\bar{C}(v_i, v_j) = \frac{1}{N(v_i)N(v_j)} \sum_{k=1}^{N(v_i)} \sum_{l=1}^{N(v_j)} C(s_k, s_l), s_k \in v_i, s_l \in v_j \quad (3)$$

$$\bar{C}(v_i, x) = \frac{1}{N(v_i)} \sum_{k=1}^{N(v_i)} C(s_k, x), s_k \in v_i \quad (4)$$

where $N(v_i)$ is the number of predicted sites contained in pixel v_i , $C(s_k, s_l)$ is the covariance between predicted site s_k of low-resolution pixel v_i and predicted site s_l of low-resolution pixel v_j , and $C(s_k, x)$ is the covariance between predicted site s_k of low-resolution pixel v_i and the current predicted site x .

3.2 Precipitation estimation merging the IMERG-based and ground observation-based hourly precipitation data

(1) Error correction based on PDF matching

PDF is an effective method to remove system

deviations, and it has been extensively applied in the error corrections of non-independent satellite data with deviations (Turk et al. 2003; Huffman et al. 2003; Wang et al. 2007; Xie et al. 2011; Shen et al. 2014).

The main idea underlying the PDF error correction of satellite precipitation data is that the probability density based on ground precipitation observations is used to calibrate the probability density of satellite precipitation estimates. This treatment aims to match the corrected probability density of satellite precipitation estimates with that based on ground precipitation observations, thereby removing the system deviations of satellite precipitation estimates. The detailed PDF error correction process is described as follows:

1) Suitable time and space windows were selected for each IMERG precipitation grid, and matching ground observations and satellite precipitation grid data were collected. Considering a high probability of zero precipitation and a small spatiotemporal scale of hourly precipitation and to ensure the acquisition of a stable probability density, with the IMERG precipitation grid to be corrected (hereafter referred to as the current grid) as the center, effective grid data pairs were selected for the time window based on a spatial window of $4^{\circ} \times 4^{\circ}$. Considering the diurnal variation characteristics, based on the current time, 20 d prior to the current date and 6 hours prior to the current time were selected as the time windows; that is, for each hourly correction, a total of 120 hourly matches of the effective grids within the $4^{\circ} \times 4^{\circ}$ spatial window where the current grid located were selected as the to-be-corrected samples. The matched ground observations and satellite precipitation collected were subjected to PDF corrections according to the procedure described in the literature (Shen et al. 2014).

2) The values of the grids whose spatiotemporal windows contained observation stations and did not lose both ground observations and satellite precipitation data were included in the statistics. The weight of each sample was calculated according to the spatial distance from the target grid and the time interval from the target time, and the samples were reordered according to their weights to determine the most effective samples.

3) The cumulative probability density of the satellite precipitation value in each grid (R_s) and the ground precipitation corresponding to the probability density (R_o) were calculated to obtain the corrected

value (Δr). The postcorrection satellite precipitation value (R_c) is calculated as $R_c = R_s + \Delta r$.

(2) OI

Among the various interpolation methods, OI, which takes the precipitation ratio into consideration, is advantageous in the spatial interpolation of precipitation (Xie et al. 2011). In the OI analysis in this study, the IMERG precipitation after the deviation correction was taken as the initial estimation field, the observed measurements at the stations were taken as the true values, and the final precipitation analysis value in each grid A_k was equivalent to the sum of the initial estimated value at this grid F_k and the deviation between the observed measurement and the initial estimated value at this grid. This deviation was obtained after the weighted estimation of the deviations between the observed measurements O_i and the initial estimated values F_i at n grids within a certain range and is described as follows:

$$A_k = F_k + \sum_{i=1}^n W_i (O_i - F_i) \quad (5)$$

where k is the analyzed grid, i is the “valid grid” (each satellite precipitation grid corresponded to at least one meteorological station), and W_i is the weight function, which represents the weight allocated in the estimation of the deviation between the observed measurement and the initial estimated value at point i . Notably, in regions with a sparse distribution of stations, the analytical radius should be continuously adjusted to ensure that a certain number of valid grids can be searched in this region; from these grids, several valid grids closest to the analyzed grid can then be selected for OI. The weight function W_i in Eq. (5) was determined by the minimum error variance in the precipitation value A_k at the analyzed point:

$$E^2 = \overline{(A_k - T_k)^2} \quad (6)$$

where T_k is the true value at point k .

Assuming no deviation between the observed measurements and the initial estimation field and that the errors of the observations were not related to those of the initial estimation field, the weight function W_i in Eq. (5) can be obtained based on the following equation:

$$\sum_{j=1}^n (\mu_{ij}^f + \mu_{ij}^o \lambda_i \lambda_j) W_j = \mu_{ki}^f \quad (7)$$

where μ_{ij}^f is the error co-correlation of the initial estimation field, μ_{ij}^o is the observation error co-correlation, and λ_i represents the ratio between the

standard deviation of the observation errors σ_i^o and that of the initially estimated errors at point i . For the sake of the solution of W_i in OI, μ_{ij}^f , μ_{ij}^o , σ_i^o and σ_i^f must all be known quantities; therefore, the error of the ground observations and that of the satellite-retrieved precipitation, as well as the correlation between them, should be preliminarily estimated. These quantities are generally given in statistical methods.

Based on Eq. (7), the weight function W_i was determined, and the final precipitation analysis value A_k was obtained based on Eq. (5).

3.3 Assessment of the merged precipitation estimates

The observed measurements at stations were taken as the precipitation ground truth. In this study, the accuracy of the merged precipitation product was assessed based on independent stations at an hourly scale using 10-fold cross-validation, the results of which were further compared with the assessment outcome of the original IMERG hourly precipitation. Primarily, 7 statistical indices were selected for the assessment. These indices fell within four categories: 1) category I, the correlation coefficient (CC) and Nash-Sutcliffe efficiency (NSE), which reflected the degree of consistency between the merged precipitation and the observed measured precipitation; 2) category II, the mean error (ME), relative bias (RB) and root mean squared error (RMSE), which described the size of the error in the merged precipitation compared with the observed measurement; 3) category III, the probability of detection (POD), false alarm ratio (FAR) and critical success index (CSI), which described the ability of the merged product to capture precipitation events; and 4) category IV, the Kling-Gupta efficiency (KGE), which is a synthetic index composed of the CC (r), deviation rate (β) and variation rate (γ). The calculations were based on Eqs. (8)–(16):

$$CC = \frac{\sum_{i=1}^n (x_i - \bar{x})(y_i - \bar{y})}{\sqrt{\sum_{i=1}^n (x_i - \bar{x})^2 \sum_{i=1}^n (y_i - \bar{y})^2}} \quad (8)$$

$$NSE = 1 - \frac{\sum_{i=1}^n (x_i - y_i)^2}{\sum_{i=1}^n (x_i - \bar{x})^2} \quad (9)$$

$$ME = \frac{1}{n} \sum_{i=1}^n (x_i - y_i) \quad (10)$$

$$PBIAS = \frac{\sum_{i=1}^n (x_i - y_i)}{\sum_{i=1}^n y_i} \times 100\% \quad (11)$$

$$RMSE = \sqrt{\frac{1}{n} \sum_{i=1}^n (x_i - y_i)^2} \quad (12)$$

$$POD = \frac{NA}{NA + NC} \quad (13)$$

$$FAR = \frac{NB}{NA + NB} \quad (14)$$

$$CSI = \frac{NA}{NA + NB + NC} \quad (15)$$

$$KGE = 1 - \sqrt{(r-1)^2 + (\beta-1)^2 + (\gamma-1)^2} \quad (16)$$

where $\bar{x} = \frac{1}{n} \sum_{i=1}^n x_i$, $\bar{y} = \frac{1}{n} \sum_{i=1}^n y_i$, n is the sample size,

and x_i and y_i are the estimated values of the merged precipitation and the observed value at the meteorological station, respectively. NA, NB and NC are the times of the accurate prediction, vacancy forecast and omission of satellite precipitation, respectively. In this study, the hourly rain/no-rain threshold was set to 0.1 mm

4 Results and Discussion

4.1 Overall assessment

Using 10-fold cross-validation and based on the observed hourly precipitation data in the Tianshan Mountains area in the warm season (May to September) of 2016–2018, we assessed the original IMERG data (OIMERG), downscaled data (DIMERG) and merged precipitation (MIMERG). Their accuracy was assessed by comparing the observed value at each station with the corresponding satellite-estimated precipitation, based on which the precision of the three sets of estimated data in the whole investigated area was comprehensively analyzed. The testing results of OIMERG, DIMERG and MIMERG based on the rain gauge-observed measurements are summarized in Table 1. The differences between DIMERG and OIMERG were small in terms of all statistical indices, which indicate that the primary

contribution of ATPK is to increase the spatial resolution of OIMERG, while it has a minor effect on the data accuracy. Then, we merged the DIMERG data with the rain gauge-based observations using the PDF-OI method and obtained the 1-km resolution merged precipitation product (MIMERG). As shown in Table 1, MIMERG was improved in all indices, particularly CC and CSI, which increased from 0.30 and 0.24 to from 0.63 and 0.38, respectively, and RMSE decreased from the original 0.46 mm to 0.38 mm. These results suggested that ATPK followed by the PDF-OI two-step correction method not only improved the spatial resolution but also increased the precision of precipitation estimation.

Fig. 2 shows the scatter plots of the overall precipitation of all the data samples and the observed precipitation from 2016 to 2018. In this figure, the rows of the panels indicate different time segments, while the columns indicate different precipitation estimation products. As shown in this figure, the scatters of the three products in different time segments were basically consistent. The data points of OIMERG and DIMERG were relatively scattered, whereas those of MIMERG were more concentrated and were distributed on both sides of the 1:1 line. These results indicated that the MIMERG data were better correlated with the observed data than any other product.

Fig. 3 presents Taylor graphs comparing the outcomes of the three products with those of the rain gauge-based data. A Taylor graph (Taylor 2001) is a diagrammatic method for comprehensively assessing the accuracy of a model (or estimation). Based on the CC and RMSE, and standard deviation (SD), this method

can quantify the consistency between a model (or an estimation) and observed values. A closer distance of the satellite estimation to the letter A (the observed data) indicates a better estimation effect. Taylor graphs are very helpful in assessing multiple complex

Table 1 Overall estimation outcomes for the OIMERG, DIMERG and MIMERG precipitation products at the hourly scale from May to September during 2016–2018 over the Tianshan Mountains.

Product	CC	RMSE (mm/h)	ME (mm/h)	POD	FAR	CSI
OIMERG	0.30	0.46	0.06	0.50	0.69	0.24
DIMERG	0.29	0.47	0.07	0.51	0.70	0.23
MIMERG	0.63	0.38	0.05	0.65	0.52	0.38

Note: OIMERG, DIMERG and MIMERG represent the original, downscaled and merged IMERG data, respectively.

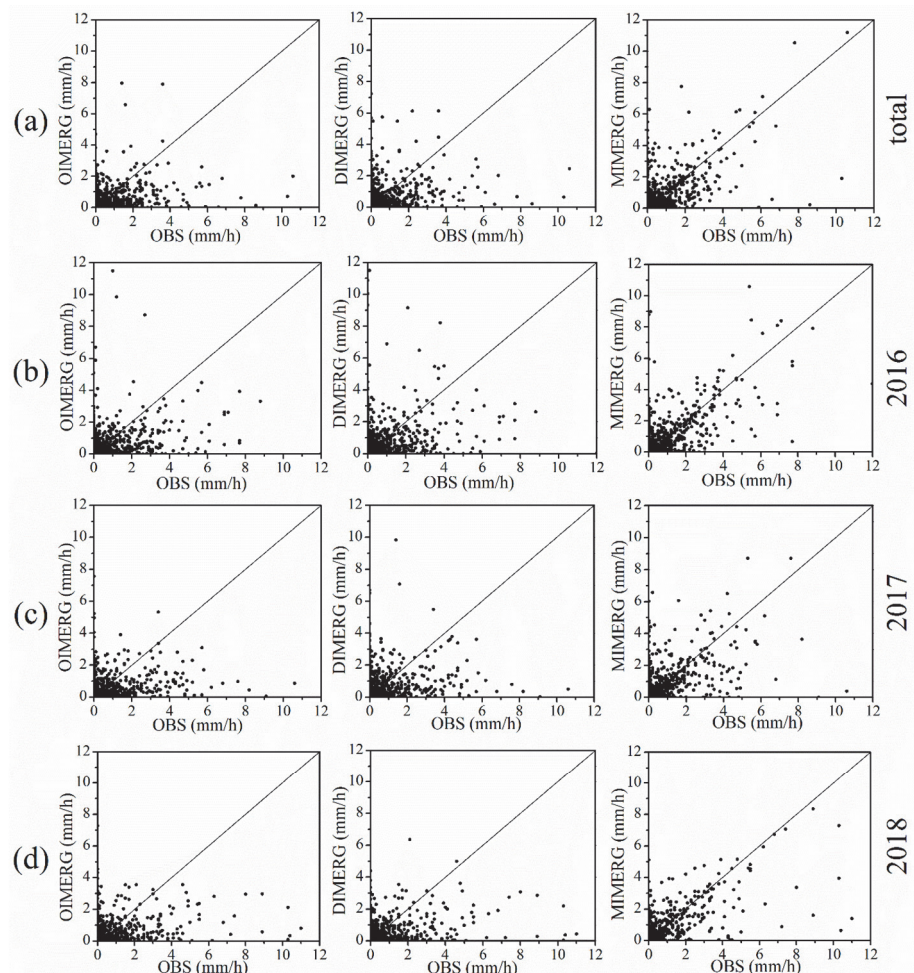


Fig. 2 Scatter plots of OIMERG, DIMERG and MIMERG compared with the observed hourly precipitation values at all stations for (a) the whole period and (b-d) each year (2016–2018) from May to September over the Tianshan Mountains (the dotted lines are 1:1 lines). Note that OBS, OIMERG, DIMERG and MIMERG represent the observed data, original IMERG, downscaled IMERG and merged IMERG, respectively.

models or measuring the performances of different models (Tang et al. 2016). Fig. 3 shows the comprehensive assessment outcomes of all the samples, OIMERG (letter B), DIMERG (letter C) and MIMERG (letter D) in 2016–2018. By integrating these three indices into a single graph, the advantages and disadvantages of each estimation product can be visually and objectively reflected. As shown in this figure, the SDs of the observed data (letter A) were 0.47, 0.61, 0.37, and 0.38 mm/h, and among the three estimation products, the SDs of MIMERG (0.42, 0.58, 0.31 and 0.31 mm/h, respectively) were the closest to those of the observed data, whereas the remaining products exhibited varying differences. In terms of the CC and RMSE, MIMERG showed the closest outcomes to the observed data. In addition, the comprehensive assessment further showed that the distance of MIMERG (letter D) to the observed measurements (letter A) was the shortest among the products, which indicated that MIMERG have the best estimation effect.

4.2 Spatial evaluation

To further reflect the distributions of the assessment indices, all assessment data of the investigated area were included in the statistics. The nine assessment indices after 10-fold cross-validation, i.e., NSE, PBIAS, KGE, CC, ME, RMSE, POD, FAR and CSI, were integrated into boxplots (Fig. 4). Boxplots describe data based on five statistical variables of a group of data, i.e., the 5th percentile, the first quartile, the median, the third quartile and the 95th percentile. Boxplots can reflect the distribution information of the data, such as the symmetry and dispersion. Overall, Fig. 4 shows that MIMERG

outperformed the other products in the nine indices, among which the NSE, KGE, CC, POD and CSI were more concentrated in the upper region, the RMSE and FAR were more concentrated in the lower region, and the PBIAS and ME were uniform on both sides of the zero-horizontal line. Specifically, the median NSE, KGE, CC, POD and CSI of MIMERG were higher (0.27, 0.38, 0.6, 0.66, and 0.4, respectively) than those of OIMERG (0.06, 0.13, 0.4, 0.5, and 0.3) and DIMERG (0, 0.1, 0.4, 0.5, and 0.3), while the median RMSE and FAR of MIMERG (0.3 and 0.5, respectively) were lower than those of OIMERG (0.4 and 0.7) and DIMERG (0.43 and 0.7). Moreover, the distributions of the PBIAS and ME of MIMERG were close to zero, exhibiting satisfactory symmetry; furthermore, the first/third quartile values were the lowest among the three products. The outcomes of this overall assessment showed that the obtained merged precipitation data after ATPK downscaling and PDF-OI correction

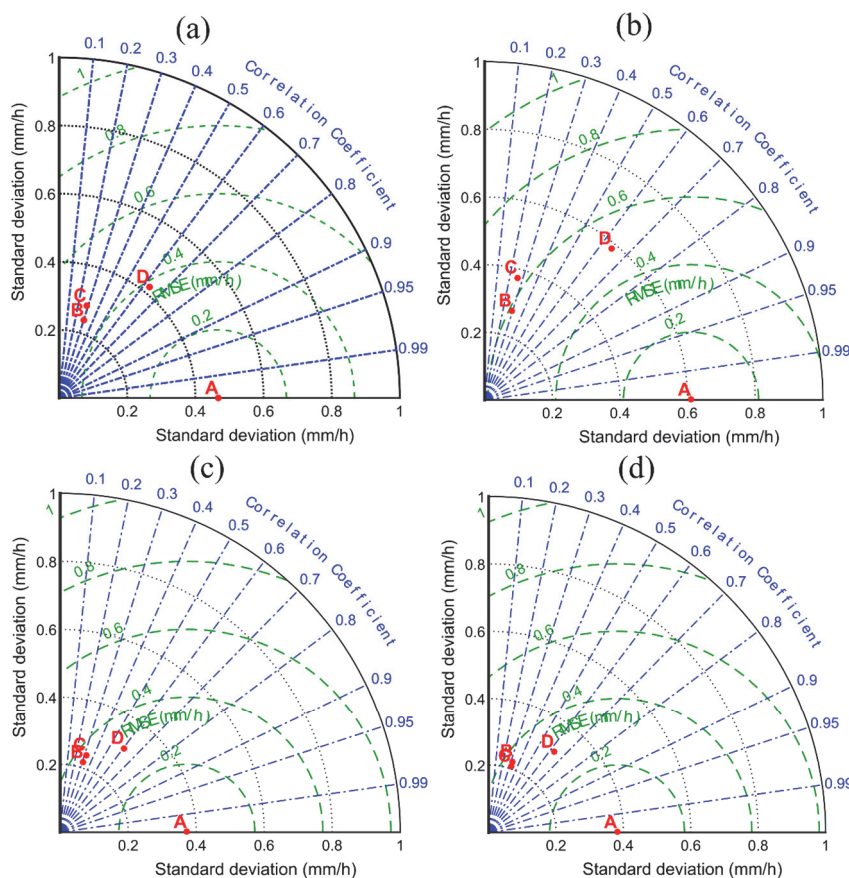


Fig. 3 Taylor graphs of the three precipitation products (OIMERG, DIMERG and MIMERG) for (a) the whole period and (b)-(d) each year (2016–2018) from May to September over the Tianshan Mountains. A: OBS; B: OIMERG; C: DIMERG; D: MIMERG. Note that OBS, OIMERG, DIMERG and MIMERG represent the observed data, original IMERG, downscaled IMERG and merged IMERG, respectively.

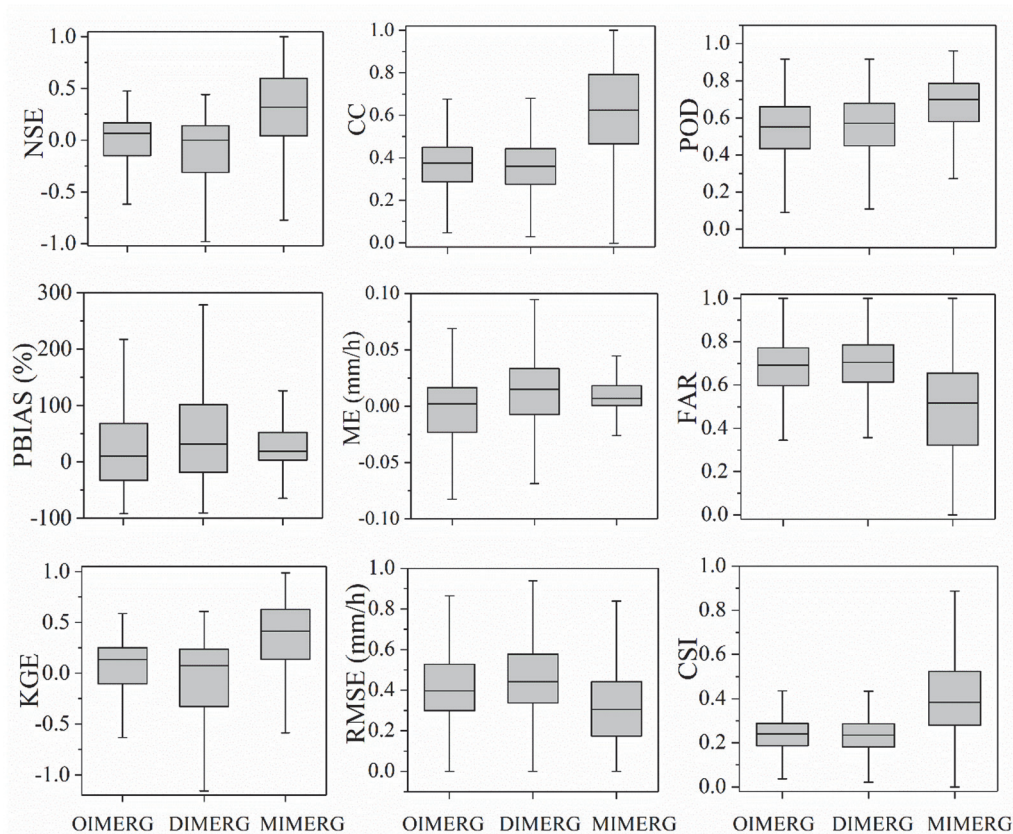


Fig. 4 Box plots of the nine indices (NSE, PBIAS, KGE, CC, ME, RMSE, POD, FAR, and CSI) for the OIMERG, DIMERG and MIMERG precipitation products at the hourly scale from May to September during 2016–2018 over the Tianshan Mountains. Note that OIMERG, DIMERG and MIMERG represent the original, downscaled and merged IMERG data, respectively.

greatly outperformed the original OIMERG and downscaled DIMERG satellite precipitation products, indicating that the method proposed in this study, i.e., increasing the spatial resolution of the original satellite precipitation product followed by merging with observed precipitation data, was feasible.

Fig. 5 shows the spatial distributions of the CC, RMSE, ME and CSI at each station in the investigated area. Overall, the spatial distributions of these indices in OIMERG were similar to those in DIMERG in both the high-value regions and the low-value regions. These results were consistent with the outcomes of the overall assessment provided in Table 1. MIMERG exhibited improvements in terms of all these indices. The CC values of OIMERG and DIMERG were basically below 0.4, whereas the CC values after merging with observed precipitation data (MIMERG) at most stations increased above 0.4. In terms of the RMSE, the number of stations whose precipitation was 0–0.2 mm/h according to MIMERG was noticeably greater than that according to OIMERG and DIMERG, whereas that of stations whose

precipitation was 0.4–0.6 mm/h according to MIMERG was noticeably lower. This difference became more obvious in the Ili River valley and eastern regions. OIMERG and DIMERG both overestimated the ME in the high-altitude regions on both the southern and the northern sides of the Tianshan Mountains but underestimated the ME in the low-altitude regions. MIMERG effectively reduced the degrees of overestimation and underestimation of OIMERG and DIMERG, and the ME values at most stations were within ± 0.025 mm/h according to MIMERG. The CSI values of OIMERG and DIMERG were less than 0.2 at nearly half of the stations, with those at the remaining stations below 0.4. In MIMERG, the number of stations whose CSI values were within the range of 0–0.2 was greatly reduced, and the CSI values at most stations increased to 0.4 and above. The spatial distributions of these assessment indices suggested that the obtained MIMERG product after ATPK downscaling and PDF-OI merging outperformed the other satellite precipitation products, which validated the high-

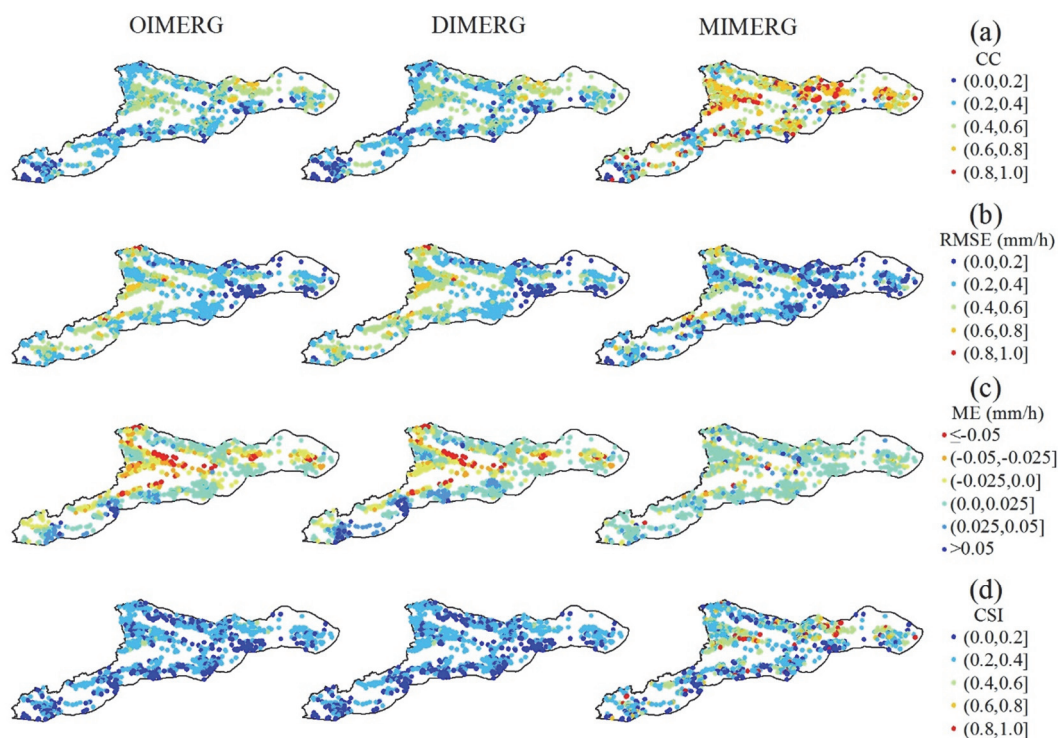


Fig. 5 Spatial distributions of the (a) CC, (b) RMSE, (c) ME, and (d) CSI values for the three satellite precipitation products (OIMERG, DIMERG, and MIMERG) at the hourly scale from May to September during 2016–2018 over the Tianshan Mountains. Note that OIMERG, DIMERG and MIMERG represent the original, downscaled and merged IMERG data, respectively.

resolution precipitation estimation algorithm proposed in this study.

4.3 Case study

From July 31 to August 1, 2016, precipitation occurred extensively from west to east in Xinjiang during the “7.31” storm, which was particularly noticeable in the Ili region. This heavy precipitation event began at 17:00 (Beijing Time) on July 31 and ended at 17:00 on August 1, and the rainfall intensity peaked at approximately 02:00 on August 1. As an example, Fig. 6 shows the assessment outcome of the merged precipitation product in terms of the spatial distribution of precipitation during this event. Figs. 6b, 6c and 6d show the precipitation distributions at 03:00 on August 1 according to the AWS observations in OIMERG, DIMERG and MIMERG, respectively. According to the ground observations, the precipitation was mainly concentrated in the Ili, Bozhou and Tacheng regions, with the large values centered in the Ili region (Fig. 6a). The Ili Valley is surrounded by mountains on three sides, forming a trumpet-shaped valley that tapers to the east. Under

the influence of water vapor from the Pacific, warm and humid air rises in the upwind direction, causing topographic-induced precipitation. Therefore, the Ili Valley is warm and humid with abundant rainfall, which is conducive to the growth of vegetation. Compared with the OBS outcome, Fig. 6b shows that the OIMERG satellite-retrieved precipitation noticeably underestimated the precipitation in the Ili region; in addition, the precipitation region according to OIMERG was far larger than the observed extent of precipitation, and the center of large values deviated to the east and north compared with the observed center. The DIMERG product (i.e., the precipitation grid product after ATPK downscaling) showed a variation tendency consistent with that of OIMERG but yielded a more precise precipitation distribution than OIMERG (Fig. 6c). In contrast, Fig. 6d shows the outcome of the MIMERG merged precipitation, which was obtained after the ATPK downscaling and PDF-OI deviation correction. MIMERG increased the spatial resolution of the original satellite precipitation and ensured the consistency of the values between the estimates in regions with observation stations and the actual AWS-measured data while maintaining the

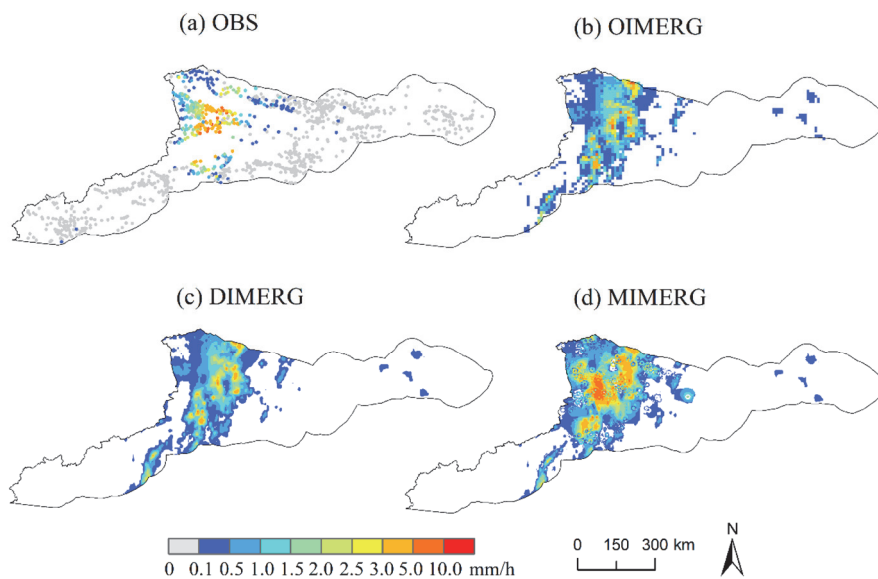


Fig. 6 Hourly precipitation (mm/h) at 03:00 (UTC+8) on August 3, 2016, over the Tianshan Mountains: (a) OBS; (b) OIMERG; (c) DIMERG; (d) MIMERG. Note that OBS, OIMERG, DIMERG and MIMERG represent the observed data, original IMERG, downscaled IMERG and merged IMERG, respectively.

satellite-retrieved precipitation distribution in the regions without observation stations. Therefore, MIMERG effectively combines the merits of the two observation methods (i.e., satellite retrievals and ground observations).

5 Discussion

5.1 The advantage of ATPK

ATPK, a downscaling method that interpolates data from known points to unknown points (Liang et al. 2015), has an important property—quality assurance; that is, the interpolation to the average of the sum of all points in any known surface is equal to the original value of the known surface. This property shows that ATPK is a downscaling method that fully retains the original data information. As a consequence, over the past decade, the ATPK geostatistical downscaling method has rapidly developed in a variety of fields, including soil science (Goovaerts 2010), medical geography (Kerry et al. 2012), remote sensing image downscaling (Peter 2013; Wang et al. 2015, 2016; Zhang et al. 2017), and satellite precipitation products (Park et al. 2017; Chen et al. 2018). In this study, ATPK was applied to atmospheric variables from previous image processing downscaling technology. Nevertheless,

although previous studies (Park et al. 2017; Chen et al. 2018) demonstrated the effectiveness of applying the ATPK method to satellite precipitation products, these researchers applied downscaling to monthly precipitation products. In contrast, this study conducted experiments on hourly precipitation products to provide high-spatiotemporal-resolution precipitation grid data to study the occurrence and development mechanism of meso- and small-scale weather systems. The introduction of the ATPK method improves the spatial

resolution of satellite precipitation data without losing the original information and thus not only achieves the downscaling of satellite precipitation products but also ensures better spatial matching between satellite precipitation data and measured observations, thereby laying a good data foundation for further merging.

5.2 Error feature analysis of OI

Compared with other merging methods for precipitation data, OI is advantageous in that it considers the autocorrelation of each type of observation error as well as the correlations between different types of observations; with this merit, the weight function is no longer limited to a univariate distance relation. In addition, the interactions between the errors caused by different types of observations are also considered. Furthermore, OI solves for the optimum value within only a certain radius of the point to be analyzed, which is particularly suitable for the analysis of single variables with a large spatiotemporal variation rate such as precipitation. To calculate the OI, the key is to determine the weight value. Thus, multiple error parameters should be calculated first, which requires preliminarily estimating the errors between the satellite-retrieved precipitation and ground observations, and the error correlation must be

determined. For example, Fig. 7 shows a scatter plot of the MSEs and rainfall intensities of the satellite-retrieved precipitation from June to August 2016. As shown in the figure, the error of the satellite-retrieved precipitation exponentially increased with increasing rainfall intensity. In addition, the correlation between the errors in the satellite estimates and those in the observed measurements at two random valid grids was plotted against the distance between the grids, yielding the error-related curve of the initial estimation field (Fig. 8). As shown in Fig. 8, the precipitation exhibited remarkable geostatistical features, where a closer distance indicated a better correlation, and vice versa. Data with different temporal resolutions have different error features. Furthermore, the thresholds set for spatiotemporal windows of different spatial resolutions were different. Considering these issues, further studies on deeper and more detailed analyses of error structures are necessary to acquire more precise precipitation estimates; i.e., the spatial window parameters of OI need to be continuously debugged or dynamically assigned according to the distribution density of stations around the current grid points to obtain the best correction effect.

5.3 Selection of auxiliary information

This study was carried out on an hourly scale. In addition to gauged precipitation data, previous studies (Immerzeel et al. 2009; Jia et al. 2011; Xu et al. 2015; Ma et al. 2017; Chen et al. 2018; Zhang et al. 2018) employed vegetation indices, terrain data, and other relevant auxiliary information for satellite data downscaling and correction. However, these studies focused mainly on relatively large time scales, such as the yearly and monthly scales, while on smaller (e.g., hourly) time scales, the correlations between precipitation and these auxiliary variables are relatively poor (Yang and Luo 2014a; Lu et al. 2018); thus, it is easy to introduce additional errors in the downscaling and correction processes, which increases the uncertainty in the results. Nevertheless, due to the limited information introduced, the downscaling and correction of satellite precipitation with only gauged precipitation data were restricted to some extent. This study used a geostatistical downscaling method to analyze hourly scale precipitation. In future research, we will try to introduce auxiliary information that can explain the

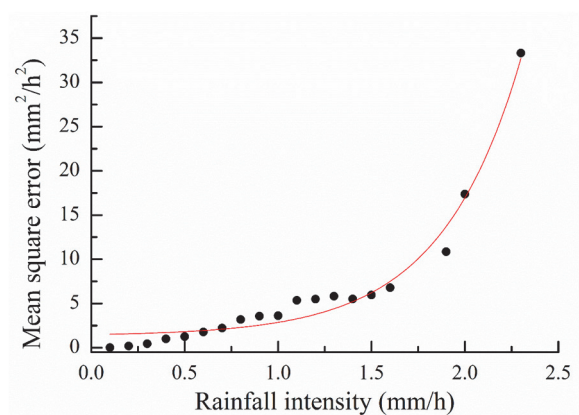


Fig. 7 MSEs of the IMERG data under different rainfall intensities.

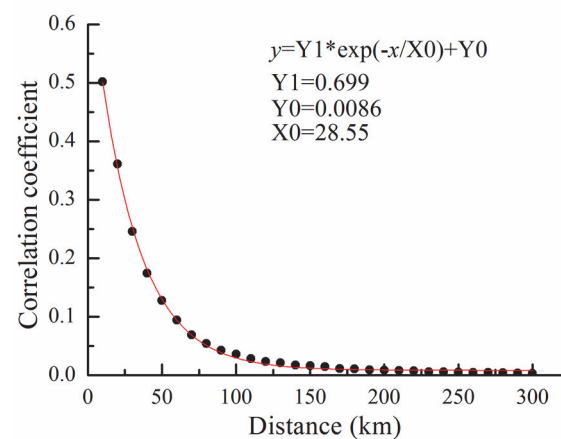


Fig. 8 Error correlation for the bias-corrected IMERG product as a function of the separation distance between two grid boxes.

variation in hourly scale precipitation to improve the prediction accuracy, and we will continue to explore the use of deep learning and other methods to jointly investigate observations from groups of stations and satellite- and radar-derived data to more accurately estimate precipitation.

6 Conclusions

In this study, based on hourly precipitation data from May to September of 2016–2018 in the Tianshan Mountains provided by 1065 regional AWSs in combination with the new-generation GPM IMERG satellite precipitation product, we proposed a method comprising ATPK downscaling followed by a PDF-OI two-step correction for research on the merging of multisource precipitation data in a mountainous region. This study led to the following conclusions.

(1) ATPK downscaling effectively increased the spatial resolution of the original IMERG satellite precipitation product without forfeiting data. A comparison between the data before and after downscaling using the observed data as the reference did not show significant differences in statistical indices.

(2) The PDF-OI results showed an increased spatial resolution and a greatly improved accuracy. A cross-validation experiment showed that the CC, POD, and CSI after PDF-OI increased from 0.30, 0.50 and 0.24 to 0.63, 0.65 and 0.38, respectively, and the RMSE, ME and FAR decreased from 0.46 mm/h, 0.06 mm/h and 0.69 to 0.38 mm/h, 0.05 mm/h and 0.52, respectively.

(3) Spatial distribution analysis showed that MIMERG effectively combined satellite precipitation estimates with gauged precipitation observations. For the areas without ground observations, the satellite precipitation data were used as the primary data. In addition, the final obtained merged precipitation product increased the resolution from the original ~10 km to 1 km, which enabled MIMERG to more precisely depict the precipitation structure.

References

- Arulraj M, Barros AP (2019) Improving quantitative precipitation estimates in mountainous regions by modelling low-level seeder-feeder interactions constrained by global precipitation measurement dual-frequency precipitation radar measurements. *Remote Sens Environ* 231: 111213. <https://doi.org/10.1016/j.rse.2019.111213>
- Baik J, Park J, Ryu D, et al. (2016) Geospatial blending to improve spatial mapping of precipitation with high spatial resolution by merging satellite-based and ground-based data. *Hydrol Process* 30: 2789–2803. <https://doi.org/10.1002/hyp.10786>
- Boushaki FI, Hsu KL, Sorooshian S, et al. (2009) Bias adjustment of satellite precipitation estimation using ground-based measurement: a case study evaluation over the southwestern United States. *J Hydrometeorol* 10: 1231–1242. <https://doi.org/10.1175/2009JHM1099.1>
- Chen X, Long D, Hong Y, et al. (2017) Improved modeling of snow and glacier melting by a progressive two-stage calibration strategy with GRACE and multisource data: How snow and glacier meltwater contributes to the runoff of the Upper Brahmaputra River basin? *Water Resour Res* 53: 2431–2466. <https://doi.org/10.1002/2016WR019656>
- Chen YY, Huang JF, Sheng SX, et al. (2018) A new downscaling-integration framework for high-resolution monthly precipitation estimates: combining rain gauge observations, satellite-derived precipitation. *Remote Sens Environ* 214: 154–172. <https://doi.org/10.1016/j.rse.2018.05.021>
- Chiang YM, Hao R, Quan S, et al. (2021) Precipitation assimilation from gauge and satellite products by a Bayesian method with Gamma distribution. *Int J Remote Sens* 42: 1017–1034. <https://doi.org/10.1080/01431161.2020.1823037>
- Gjertsen U, Dahl JI (2002) Challenges for precipitation estimation in mountainous regions. *Radar Meteorol (ERAD)*, 250–254.
- Goovaerts P (2010) Combining areal and point data in geostatistical interpolation: applications to soil science and medical geography. *Math Geosci* 42: 535. <https://doi.org/10.1007/s11004-010-9286-5>
- Han PF, Long D, Han ZY, et al. (2019) Improved understanding of snowmelt runoff from the headwaters of China's Yangtze River using remotely sensed snow products and hydrological modeling. *Remote Sens Environ* 224: 44–59. <https://doi.org/10.1016/j.rse.2019.01.041>
- Han ZY, Long D, Han PF, et al. (2021) An improved modeling of precipitation phase and snow in the Lancang River Basin in Southwest China. *Sci China Technol Sc* 64: 1513–1527. <https://doi.org/10.1007/s11431-020-1788-4>
- Immerzeel WW, Rutten M, Droogers P, et al. (2009) Spatial downscaling of TRMM precipitation using vegetative response on the Iberian Peninsula. *Remote Sens Environ* 113: 362–370. <https://doi.org/10.1016/j.rse.2008.10.004>
- Jia SF, Zhu WB, Lv AF, et al. (2011) A statistical spatial downscaling algorithm of TRMM precipitation based on NDVI and DEM in the Qaidam Basin of China. *Remote Sens Environ* 115: 3069–3079. <https://doi.org/10.1016/j.rse.2011.06.009>
- Jin Y, Ge Y, Wang JH, et al. (2018) Geographically weighted area-to-point regression kriging for spatial downscaling in remote sensing. *Remote Sens* 10(4): 579. <https://doi.org/10.3390/rs10040579>
- Kidd C, Huffman GJ (2011) Global Precipitation Measurement. *Meteorol Appl* 18: 334–353. https://doi.org/10.1007/978-3-540-77655-0_6
- Kiyomars R and Farhad A (2018) A multiscale spatio-temporal framework to regionalize annual precipitation using k-means and self-organizing map technique. *J Mt Sci* 15: 1481–1497. <https://doi.org/10.1007/s11629-017-4684-5>
- Kyriakidis PC (2004) A geostatistical framework for area-to-point spatial interpolation. *Geogr Anal* 36: 259–289. <https://doi.org/10.1111/j.1538-4632.2004.tb01135.x>
- Kyriakidis PC, Yoo EH (2005) Geostatistical Prediction and Simulation of Point Values from Areal Data. *Geogr Anal* 37(2): 124–151.
- Huffman GJ, Adler RF, Stocker EF, et al. (2003) Analysis of TRMM 3-hourly Multi-satellite Precipitation Estimates Computed in Both

- Real Time and Post-real Time. 12th Conf on Satellite Meteorology and Oceanography, AMS.
- Kerry R, Goovaerts P, Rawlins BG, et al. (2012) Disaggregation of legacy soil data using area to point kriging for mapping soil organic carbon at the regional scale. *Geoderma* 170: 347–358. <https://doi.org/10.1016/j.geoderma.2011.10.007>
- Li M, Shao QX (2010) An improved statistical approach to merge satellite rainfall estimates and rain gauge data. *J Hydrol* 385: 51–64. <https://doi.org/10.1016/j.jhydrol.2010.01.023>
- Liang YZ, Ge Y, Wang Jh, et al. (2015) Review of Geostatistical-based Downscaling. *Remote Sens Tech Appl* 30(1): 1-7. (In Chinese) <https://doi.org/10.11873/j.issn.1004-0323.2015.1.0001>
- Liu XH, Kyriakidis PC, Goodchild MF et al. (2008) Population - density estimation using regression and area - to - point residual kriging. *Int J Geogr Inf Sci* 22: 431–447. <https://doi.org/10.1080/13658810701492225>
- Lu XY, Tang GQ, Wei M, et al. (2018a) Evaluation of multi-satellite precipitation products in Xinjiang, China. *Int J Remote Sens* 39(21): 7437-7462. <https://doi.org/10.1080/01431161.2018.1471246>
- Lu XY, Wei M, Tang GQ, et al. (2018b) Evaluation and correction of the TRMM 3B43V7 and GPM 3IMERGM satellite precipitation products by use of ground-based data over Xinjiang, China. *Environ Earth Sci* 77: 209. <https://doi.org/10.1007/s12665-018-7378-6>
- Ma ZQ, Shi Z, Zhou Y, et al. (2017) A spatial data mining algorithm for downscaling TMPA 3B43 V7 data over the Qinghai–Tibet Plateau with the effects of systematic anomalies removed. *Remote Sens Environ* 200: 378–395. <https://doi.org/10.1016/j.rse.2017.08.023>
- Marquinez J, Lastra J, Garcia P (2003) Estimation models for precipitation in mountainous regions: the use of GIS and multivariate analysis. *J Hydrol* 270(1-2): 1-11. [https://doi.org/10.1016/S0022-1694\(02\)00110-5](https://doi.org/10.1016/S0022-1694(02)00110-5)
- Nan Y, Nicolas G, Pierre T (2018) Polarimetric x - band weather radars for quantitative precipitation estimation in mountainous regions. *Q J Roy Meteor Soc* 144: 717. <https://doi.org/10.1002/qj.3366>
- Park NW, Kyriakidis PC, Hong S (2017) Geostatistical integration of coarse resolution satellite precipitation products and rain gauge data to map precipitation at fine spatial resolutions. *Remote Sens* 9: 255. <https://doi.org/10.3390/rs9030255>
- Qi YC, Min JZ, Zhang J, et al. (2010) Radar-based Quantitative Precipitation Estimation for the Cool Season in Mountainous Regions. WMO International Conference on Quantitative Precipitation Estimation & Quantitative Precipitation Forecasting & Hydrology.
- Shen Y, Zhao P, Pan Y, et al. (2014) A high spatiotemporal gauge-satellite merged precipitation analysis over China. *J Geophys Res-Atmos* 119: 3063-3075. <https://doi.org/10.1002/2013JD020686>
- Shen Y, Hong Z, Pan Y, et al. (2018) China's 1 km Merged Gauge, Radar and Satellite Experimental Precipitation Dataset. *Remote Sens* 10(2): 264. <https://doi.org/10.3390/rs10020264>
- Tang GQ, Ma YZ, Long D et al. (2015) Evaluation of GPM Day-1 IMERG and TMPA Version-7 legacy products over Mainland China at multiple spatiotemporal scales. *J Hydrol* 533: 152-167. <https://doi.org/10.1016/j.jhydrol.2015.12.008>
- Tang GQ, Zeng ZY, Guo X, et al. (2016) Statistical and Hydrological Comparison between TRMM and GPM Level-3 Products over a Midlatitude Basin: Is Day-1 IMERG a Good Successor for TMPA 3B42V7? *J Hydrometeorol* 17: 121–137. <https://doi.org/10.1175/JHM-D-15-0059.1>
- Tang GQ, Clark MP, Papalexio SM, et al. (2021) EMDNA: Ensemble Meteorological Dataset for North America. *Earth Syst Sci Data* 13(7): 3337-3362. <https://doi.org/10.5194/essd-13-3337-2021>
- Turk FJ, Ebert EE, Oh HJ, et al. (2003) Validation of an Operational Global Precipitation Analysis at Short Time Scales. 12th Conf on Satellite Meteorology and Oceanography, American Meteorological Society.
- Verdin A, Rajagopalan B, Kleiber W, et al. (2015) A Bayesian kriging approach for blending satellite and ground precipitation observations. *Water Resour Res* 51: 908–921. <https://doi.org/10.1002/2014WR015963>
- Wang WQ, Xie PP (2007) A multiplatform-merged (MPM) SST analysis. *J Climate* 20(9): 1662-1679. <https://doi.org/10.1175/JCLI4097.1>
- Wen YX, Kirstetter PE, Gourley JJ, et al. (2014) How Spaceborne Radar can enhance ground radar network for improved understanding of precipitation rates and types over mountainous regions. 16th Conference on Mountain Meteorology American Meteorological Society.
- Wu ZY, Zhang YL, Sun ZL, et al. (2018) Improvement of a combination of TMPA (or IMERG) and ground-based precipitation and application to a typical region of the East China Plain. *Sci Total Environ* 640–641: 1165–1175. <https://doi.org/10.1016/j.scitotenv.2018.05.272>
- Xie PP, Xiong AY (2011) A conceptual model for constructing high-resolution gauge-satellite merged precipitation analyses. *J Geophys Res* 116: D21106. <https://doi.org/10.1029/2011JD016118>
- Xu SG, Wu CY, Wang L, et al. (2015) A new satellite-based monthly precipitation downscaling algorithm with non-stationary relationship between precipitation and land surface characteristics. *Remote Sens Environ* 162: 119-140. <https://doi.org/10.1016/j.rse.2015.02.024>
- Yang YF, Luo Y (2014a) Evaluating the Performance of Remote Sensing Precipitation Products CMORPH, PERSIANN, and TMPA, in the Arid Region of Northwest China. *Theor Appl Climatol* 118: 429–445. <https://doi.org/10.1007/s00704-013-1072-0>
- Yang YF, Luo Y (2014b) Using the Back Propagation Neural Network Approach to Bias Correct TMPA Data in the Arid Region of Northwest China. *J Hydrometeorol* 15(1): 459-473. <https://doi.org/10.1175/JHM-D-13-041.1>
- Yang T, Li Q, Chen X, et al. (2020) Evaluation of spatiotemporal variability of temperature and precipitation over the Karakoram Highway region during the cold season by a Regional Climate Model. *J Mt Sci* 17: 2108–2122. <https://doi.org/10.1007/s11629-019-5772-5>
- Yin ZY, Liu XD, Zhang XQ, et al. (2004) Using a geographic information system to improve Special Sensor Microwave Imager precipitation estimates over the Tibetan Plateau. *J Geophys Res-Atmos* 109: D03110. <https://doi.org/10.1029/2003JD003749>
- Yin ZY, Zhang XQ, Liu XD, et al. (2008) An Assessment of the Biases of Satellite Rainfall Estimates over the Tibetan Plateau and Correction Methods Based on Topographic Analysis. *J Hydrometeorol* 9(3): 301-326. <https://doi.org/10.1175/2007JHM903.1>
- Yu RC, Yuan WH, Li J (2013) The asymmetry of rainfall process. *Chinese Sci Bull* 58(16): 1850-1856. <https://doi.org/10.1007/s11434-012-5653-6>
- Zhang T, Li BL, Yuan YC, et al. (2018) Spatial downscaling of TRMM precipitation data considering the impacts of macro-geographical factors and local elevation in the Three-River Headwaters Region. *Remote Sens Environ* 215: 109-127. <https://doi.org/10.1016/j.rse.2018.06.004>
- Wang QM, Shi WZ, Atkinson PM, et al. (2015) Downscaling MODIS images with area-to-point regression kriging. *Remote Sens Environ* 166: 191–204. <https://doi.org/10.1016/j.rse.2015.06.003>
- Zhang YH, Atkinson PM, Ling F, et al. (2017) Spectral-spatial adaptive area-to-point regression kriging for MODIS image downscaling. *IEEE J-Stars* 10: 1883–1896. <https://doi.org/10.1109/JSTARS.2017.2650260>
- Zheng Q, Chen RS, Han CT, et al. (2018) Adjusting precipitation measurements from the TRwS204 automatic weighing gauge in the Qilian Mountains, China. *J Mt Sci* 15(11): 2365-2377. <https://doi.org/10.1007/s11629-018-4839-z>